https://doi.org/10.5194/egusphere-2026-4240
Preprint. Discussion started: 14 August 2026

Multi-Sensor Data Assimilation for Global Soil Moisture Estimation Using the Local Ensemble Transform Kalman Filter

Sunlae Tak[1,2], Eunkyo Seo[3,4], Myong-In Lee[1], Rolf H. Reichle[5]

[1]Department of Civil, Urban, Earth, and Environmental Engineering, Ulsan National Institute of Science and Technology, Ulsan, 44919, Republic of Korea
[2]Institute of Sustainable Earth and Environmental Dynamics (SEED), Pukyong National University, Busan, 48513, Republic of Korea
[3]School of Environmental Atmosphere Science, Pukyong National University, Busan, 48513, Republic of Korea
[4]Center for Ocean-Land-Atmosphere Studies, George Mason University, Fairfax, VA, 22030, United States
[5]Global Modeling and Assimilation Office, NASA Goddard Spaceflight Center, Greenbelt, MD, United States

Correspondence to: Myong-In Lee (milee@unist.ac.kr), Eunkyo Seo (eseo@pknu.ac.kr)

Abstract. This study investigates whether assimilating soil moisture (SM) observations from multiple sensors can increase spatiotemporal coverage and improve SM estimates. A global SM data assimilation (DA) system based on the Local Ensemble Transform Kalman Filter is used to merge Level-2 SM retrievals from the Soil Moisture Active Passive (SMAP) mission, the Soil Moisture and Ocean Salinity (SMOS) mission, the Advanced Scatterometer (ASCAT), and the Advanced Microwave Scanning Radiometer 2 (AMSR2) into the Joint UK Land Environment Simulator (JULES) land surface model. Retrievals are assimilated both individually and jointly over the boreal warm seasons (2015–2021). An additional experiment assimilates the gridded European Space Agency (ESA)-Climate Change Initiative (CCI) multi-satellite product to provide a benchmark comparison.

The resulting SM estimates are validated using an Instrumental Variable approach at the global scale and against in-situ observations across North America, Europe, and East Asia. The four single-sensor DA experiments result in a global average improvement of 0.045 in the anomaly correlation coefficient (R) compared to the model-only (Openloop) simulation, with SMAP assimilation yielding the highest skill over 48 % of global land areas. All single-sensor experiments improve both surface and root-zone SM estimates relative to the Openloop. The multi-sensor DA system further enhances performance, outperforming both single-sensor experiments and the assimilation of ESA-CCI products. These benefits are also evident at the sub-daily timescale. The skill improvement of the multi-sensor DA over single-sensor DA at each sub-daily time step is associated with the overpass times of the individual sensors and their respective performance. Overall, this study demonstrates that expanding the spatiotemporal coverage of satellite observations through multi-sensor assimilation provides more accurate and robust SM estimates.

https://doi.org/10.5194/egusphere-2026-4240
Preprint. Discussion started: 14 August 2026

1 Introduction

Soil moisture (SM) serves as a fundamental driver in modulating the land surface cycles of water, energy, and carbon, largely through its influence on ecosystem and land-atmosphere coupling (Barnett et al., 2005; Bateni and Entekhabi, 2012; Seneviratne et al., 2010; Trenberth et al., 2013). Furthermore, the spatiotemporal heterogeneity of SM dictates the onset and severity of droughts and floods, making accurate SM estimation vital for effective disaster monitoring and management (Berg et al., 2016; Halder and Dirmeyer, 2016; Konapala et al., 2020; Koster et al., 2004; Wu et al., 2020). Despite its importance, accurately quantifying SM on a large scale remains a significant challenge due to its high spatiotemporal variability and the limitations of conventional in-situ measurements (Koster et al., 2009; Seo and Dirmeyer, 2022a).

The inherent constraints and spatial sparsity of in-situ point measurements render gridded observational data indispensable for resolving the spatial heterogeneity of SM. This necessity has catalysed the advancement of microwave satellite remote sensing, establishing it as a robust solution for consistent, large-scale monitoring (Reichle et al., 2009; Reichle et al., 2021). Microwave signals can propagate through cloud layers and exhibit strong sensitivity to soil dielectric properties, thereby directly reflecting the volumetric soil moisture (Karthikeyan et al., 2017; Kumar et al., 2006; Liu et al., 2011). Therefore, these satellites enable the acquisition of SM estimates at the global scale.

Satellite-based SM data, however, also have several inherent limitations. The limited penetration depth of microwave sensors implies that they primarily sense the SM content within the uppermost soil layer (0~5 cm). This poses a significant challenge for understanding the moisture conditions of deeper soil layers. Furthermore, vegetation canopy and surface roughness can interfere with the microwave signal, causing it to be attenuated or scattered, thereby reducing the accuracy of satellite data in regions with particularly dense vegetation or complex terrain (Kumar et al., 2022). The physical characteristics of the sensors themselves also present challenges. For example, passive microwave sensors, while covering broad areas, typically feature a coarse spatial footprint. This makes it difficult to capture small-scale SM variability in agricultural fields or complex terrain. Conversely, active sensors offer a higher resolution but can suffer from issues like noise interference and signal saturation (Wagner et al., 2013). Due to these limitations, satellite-derived SM data contain uncertainty, and their accuracy tends to decrease in complex environments (Kim et al., 2021; Li et al., 2024; Seo and Dirmeyer, 2022b; Wagner et al., 2013). To improve the practical application and confidence in satellite SM retrievals, it is essential to mitigate these shortcomings (De Lannoy and Reichle, 2016).

Data assimilation (DA) frameworks have been widely adopted to combine observations from satellite platforms with land surface model (LSM) simulations (Nichols, 2010), which mitigates some of the inherent limitations of the satellite SM data. A DA system effectively integrates spatially and temporally heterogeneous observational data with a priori estimates from LSMs, accounting for their respective errors. This process enhances consistency under the constraints of physical conservation laws while integrating diverse observational sources (Reichle, 2008). Several studies have successfully improved SM analyses by using ensemble-based filtering techniques to assimilate observations from different satellites into

https://doi.org/10.5194/egusphere-2026-4240
Preprint. Discussion started: 14 August 2026

their respective models (De Lannoy and Reichle, 2016; Kumar et al., 2019; Liu et al., 2011; Seo et al., 2021; Beck et al., 2021).

While single-sensor DA has provided valuable insights, it is often constrained by inherent trade-offs, such as temporal gaps or coarse spatial resolution. Consequently, there is a growing consensus on the need to leverage the synergistic benefits of multiple sensors to generate a more robust, continuous, and high-resolution SM record. Early efforts, such as the assimilation of the Advanced Scatterometer (ASCAT)(Wagner et al., 2013) and the Advanced Microwave Scanning Radiometer-E (AMSR-E)(Parinussa et al., 2011a), demonstrated that combining different microwave observations could improve SM skills in the surface and root zone over the continental United States (Draper et al., 2012). Building on this, more recent studies have explored the joint utilization of active microwave backscattering and passive thermal emission. For example, Lievens et al. (2017) successfully enhanced spatial details by jointly assimilating Sentinel-1 and SM Active Passive (SMAP) mission (Entekhabi et al., 2010b) data in four regional domains, effectively merging the high-resolution of radar with the radiometric precision of radiometers. Furthermore, the benefits of multi-sensor DA extend beyond land surface modeling to hydrological applications; showed that assimilating Sentinel-1 and SMAP retrievals into the SWAT model significantly improved flood simulations in two small basins in Italy, underscoring the pivotal impact of observation frequency on the fidelity of state updates and spatial scale of the retrievals. In parallel, advancements continue in improving temporal coverage and algorithm sophistication. Kim et al. (2021) improved sub-daily skills by incorporating SMAP and Cyclone Global Navigation Satellite System (CYGNSS)(Ruf et al., 2018) SM retrievals across a quasi-global domain, while Seo et al. (2021) enhanced SM representation over North America using an advanced LETKF system integrating SMAP and ASCAT. Collectively, these studies confirm that a multi-sensor assimilation approach is essential for achieving a comprehensive characterization of terrestrial hydrology (Fox et al., 2025).

This study follows up on Seo et al. (2021) and is motivated by the question of whether incorporating additional satellite observations can further enhance the performance of the DA system. For our analysis, we leverage SM data from four operational satellite missions operating at frequencies below 10 GHz, which are best suited for sensing SM. In addition to assimilating SM from SMAP and ASCAT as in Seo et al. (2021), the present study also assimilates observations from the SM and Ocean Salinity (SMOS) mission (Kerr et al., 2012) and the Advanced Microwave Scanning Radiometer 2 (AMSR2)(Parinussa et al., 2015). Moreover, the present study extends the North America domain of Seo et al. (2021) to the global domain. While previous pioneering efforts have largely been geographically constrained to specific basins or regional domains, this study addresses this gap by implementing a multi-sensor DA framework on a truly global scale. DA is performed for the satellite observations, both individually and in combination, utilizing the LETKF. We compare the skills of both single-sensor and multi-sensor DA experiments to quantitatively assess the impact of the multi-sensor approach and to characterize the individual contributions of each sensor. This assessment extends to sub-daily timescales, allowing us to examine how increased satellite sampling frequency improves the fidelity of soil moisture state updates. In addition, we include data assimilation experiments using the European Space Agency (ESA)-Climate Change Initiative (CCI) soil

https://doi.org/10.5194/egusphere-2026-4240
Preprint. Discussion started: 14 August 2026

moisture product. a pre-merged, multi-sensor dataset, as an independent benchmark to further evaluate the benefits of the multi-sensor approach.

The paper is structured as follows. Sect. 2 details the LSM and the datasets used in this study, followed by an explanation of the assimilation methodology, preprocessing, and validation strategy. The results are presented and discussed in Sect. 3. Finally, Sect. 4 offers a summary of the key findings and conclusions.

2 Data and Method

2.1 Land surface model

This study employs the Joint UK Land Environment Simulator (JULES), a community-based LSM. The model configuration accounts for surface heterogeneity using nine land cover tiles (Best et al., 2011). The model distinguishes between five plant functional types (PFTs), such as broadleaf and needleleaf forests, and four non-vegetated categories, including urban areas and bare ground. Surface parameters such as aerodynamic roughness and albedo are assigned based on these specific land classifications. Vertically, the soil column is discretized into four layers, with bottom depths located at 0.1, 0.35, 1.0, and 3.0 m. The computational domain is spatially discretized at a horizontal grid spacing of approximately 50 km.

Given the importance of rainfall in soil moisture modeling, precipitation data are primarily obtained from the Global Satellite Mapping of Precipitation (GSMaP) product (Aonashi et al., 2009). We utilize the hourly, gauge-calibrated GSMaP rates (10 km resolution) restricted to the region between 60°S and 60°N, while relying on JRA-55 precipitation for high-latitude regions. To match the reanalysis timing, GSMaP data are aggregated into 6-hour intervals. Regarding the remaining atmospheric drivers, such as near-surface air temperature, wind speed, and specific humidity, we employ the 55-year Japanese Reanalysis (JRA-55), which offers 6-hourly data at 0.56° resolution (Kobayashi et al., 2015). Non-precipitation variables are linearly interpolated to the 1-hour model time step, and all datasets are spatially regridded to fit the JULES domain. Precipitation and radiation variables, provided as backward-averaged values, are treated as constant within each data interval. An ensemble approach is utilized to evaluate the uncertainties associated with JULES simulations, accounting for both atmospheric drivers and prognostic state variables, including radiation, rainfall, and SM, which are perturbed with random numbers to account for uncertainty (Seo et al., 2021).

2.2 Data

For the purpose of validation, this study utilizes SM data collected from various in-situ networks over North America, Europe, and East Asia from the International SM Network (ISMN) (Fig. S1 and Table S1). These in-situ observation networks provide volumetric water content monitored at the 5-cm soil level and hourly intervals, accompanied by quality flags to indicate data reliability. The 5 cm depth data are used for surface SM analysis, while root-zone SM is calculated by averaging the measurements from the 5, 10, and 20 cm depths, with each value weighted by its respective layer thickness

https://doi.org/10.5194/egusphere-2026-4240
Preprint. Discussion started: 14 August 2026

(only surface SM is available in East Asia). For this analysis, only data with a "good" quality flag are used. Observations falling outside the physically plausible limits or obtained during frozen ground states are filtered out. We then calculate 3-hourly and daily averages from the quality-controlled data to be used for verification. The validation includes only the dates for which data are available in all eight 3-hourly time intervals. Stations that provide only daily averaged observations (e.g. PBO-H2O and East Asia) are not used in the sub-daily validation.

To ensure data reliability, only stations with more than 50 days of observations during the study period are retained. Furthermore, we exclude stations where the anomaly correlation skill (against in situ measurements) of any satellite sensor is worse by at least 0.2 than the Openloop skill. This step excludes locations where satellite observations are of poor quality; future work will examine how best to integrate this a priori QC step into the DA system. When two stations fall within the same model grid cell, the assimilation estimates from this grid cell are validated separately against the two stations. Consequently, at the daily timescale we validate the surface (root-zone) SM analysis at 230 (58) stations in North America, 61 (48) stations in Europe, and 35 (0) stations in East Asia.

The validation results are classified based on land cover categories as specified by the Moderate Resolution Imaging Spectroradiometer (MODIS) Collection 5 product (Friedl et al., 2010). The categories employed in our validation are based on 17 International Geosphere–Biosphere Programme (IGBP) classifications: “Forest” consists of IGBP classes 1-5, “Shrub” consists of classes 6-7, “Savanna” consists of classes 8-9, “Grassland” consists of class 10, “Wetland” consists of class 11, “Crop” consists of classes 12 & 14, “Urban” consists of class 13, “Snow and ice” consists of class 15, and “Barren” consists of class 16 (Fig. S1). For this study, the land cover categories used include Forest, Shrub, Grassland, Crop, and Savanna.

This study assimilates SM retrievals from four sensors: SMAP, SMOS, ASCAT, and AMSR2. SMAP and SMOS are L-band passive sensors with a sampling depth of approximately ~5 cm. Both SMAP and SMOS utilize L-band brightness temperature (TB) to retrieve SM. SMAP employs a dual-channel algorithm (DCA), whereas SMOS integrates dual-polarization, multi-angular TB measurements within the L-band Microwave Emission of Biosphere (L-MEB) modeling framework. SMAP data have been available since 2015, and the DA period for this study is aligned with this timeframe (Table S2). For ASCAT, data collected by MetOp-A (05/2007–11/2021), MetOp-B (09/2012–present), and MetOp-C (11/2018–present) are assimilated. ASCAT is an active sensor and AMSR2 is a passive sensor; both are operating in the C-band and have a sampling depth of approximately ~2 cm. We further utilized version v09.2 of the ESA-CCI SM dataset (Gruber et al., 2019), which provides long-term global records by merging various passive and active microwave sensors, including the four sensors used in our DA experiments. During the period of interest, ESA-CCI v09.2 integrates passive microwave radiometers such as AMSR2, SMOS, SMAP, the Global Precipitation Measurement (GPM) Microwave Imager (GMI)(Draper et al., 2015), and Fengyun (FY)-3B/C/D (Yang et al., 2012), as well as active observations from ASCAT (PUG 2021).

SM retrievals are provided within ~25 minutes of 06:00/18:00 local time (LT) for SMAP and SMOS, 9:30/21:30 LT for ASCAT, 01:30/13:30 LT for AMSR2, while ESA-CCI provides daily mean values. The horizontal resolution is 36 km for SMAP and SMOS, 25 km for ASCAT, 10 km for AMSR2, and 25 km for ESA-CCI (Table S2). All SM retrievals are

https://doi.org/10.5194/egusphere-2026-4240
Preprint. Discussion started: 14 August 2026

regridded to the 50 km spatial resolution of the JULES simulation preceding the assimilation step. For DA, the observation error standard deviations are set as follows: 0.04 m³ m-³ for SMAP (Chan et al., 2016), 10% degree of saturation for ASCAT (Dorigo et al., 2010), and 0.08 m³ m-³ for both SMOS (Xu et al., 2015) and AMSR2 (Cho et al., 2015), and 0.025 m³ m-³ for ESA-CCI (Heyvaert et al., 2023). Satellite observations were screened based on the quality assurance flags provided within the data products. Observations over forest land cover (MODIS land cover data) with more than 60% tree and woody vegetation, wetlands covering over 10% of the grid area (referenced from ASCAT data), or topographical complexity exceeding 10% are excluded. Additionally, SM retrievals are filtered out under specific conditions: specifically under conditions where the JULES-simulated surface temperature falls below 274 K, daily rainfall accumulation exceeds 50 mm, or snow cover is present. For the SMOS sensor, quality control related to radio frequency interference (RFI) can be important. However, owing to the relatively large observation error standard deviation of 0.08 m³ m-³ used for SMOS in this study, the impact of applying RFI filtering (RFI < 10%) to SMOS observations is found to be negligible in the DA results (Fig. S6).

2.3 Local Ensemble Transform Kalman Filter

This study applies the LETKF (Hunt et al., 2007; Miyoshi and Yamane, 2007; Seo et al., 2021). Operating as a localized ensemble approach, the LETKF computes the state update independently for each computational node by incorporating measurements falling within a prescribed radius of influence, utilizing error covariances estimated from the ensemble members. This process relies on spatial localization, a critical technique that mitigates the unrealistic impact of distant observations on the analysis. Because analysis increments are only computed for surface SM analysis, a two-dimensional horizontal local patch is utilized.

In this study, the local patch is configured as a two-dimensional horizontal window measuring 150 km × 150 km, given that the analysis is limited to the top soil layer. The corresponding state vector X has dimensions of L × N, where L is the patch size and N is the ensemble size. We utilize the notations X_b and X_a to designate the prior forecast field and the updated analysis, respectively. The analyzed state vector is represented as

$$X_a = \bar{X}_a + X_a'{}' \tag{1}$$

where $\bar{X}_a$ is an L × 1 state vector denoting the mean of the posterior ensemble, and X_a' is an L × N matrix representing the deviations from the mean analysis across N ensemble members. The ensemble mean of the analysis, $\bar{X}_a$, is computed as

$$\bar{X}_a = \bar{x}_b + \delta\bar{x}_a \tag{2}$$

where $\bar{x}_b$ is the background (forecast) ensemble mean, and $\delta\bar{x}_a$ is the analysis mean increment ($L \times 1$). $\delta\bar{x}_a$ can be obtained as

$$\delta\bar{x}_a = X_b'\tilde{P}_a(Y_b')^T R^{-1} d \tag{3}$$

https://doi.org/10.5194/egusphere-2026-4240
Preprint. Discussion started: 14 August 2026

where X_b' denotes the prior ensemble anomaly matrix, $\tilde{P}_a$ is the analysis covariance within the ensemble subspace, Y_b' are the prior anomalies projected into observation space, R is the measurement error covariance, and d is the innovation vector (difference between observations and forecast).

In the LETKF formulation, covariance localization is achieved via a distance-based weighting scheme within each local domain. This ensures that proximal observations are assigned greater weight in the analysis. Specifically, this study utilizes a Gaussian weighting function:

$$w(r_i) = \exp(-r_i{}^2/2\sigma^2) \quad (4)$$

where r_i is the distance between the center of the local patch and the i-th observation, and σ is the localization scale parameter. Following previous studies, σ is set to 30 km (Seo et al. 2021). To implement distance-based localization, the weights are incorporated into the observation-error covariance as $R_w^{-1} = W^{1/2}R^{-1}W^{1/2}$, and $W = diag(w(r_i))$. Then, the analysis mean increment ($\delta\bar{x}_a$) can be obtained as

$$\delta\bar{x}_a = X_b'\tilde{P}_a(Y_b')^T R_w^{-1}(d) \quad (5)$$

$$\tilde{P}_a = [(Y_b')^T R_w^{-1}(Y_b') + (N-1)I/\rho]^{-1} \quad (6)$$

and ρ=1.2 is the covariance inflation parameter (equivalent to a 20% multiplicative inflation). It mitigates the underestimation of ensemble spread, a key cause of filter divergence, arising from assumptions characterized by spatiotemporally invariant uncertainties in both forcing inputs and observations, as well as from the limited ensemble size.

2.4 Preprocessing of satellite soil moisture observations

Differences between satellite-derived SM observations and LSM outputs arise from unresolved deficiencies in the LSM's physical parameterizations and discrepancies in the soil layer depths measured by satellite instruments. These inconsistencies introduce substantial biases between the two datasets. To mitigate systematic differences between the datasets, we employ a statistical bias correction strategy (Reichle and Koster, 2004) for aligning satellite retrievals with the model's climatological baseline. This bias correction step is executed as a preprocessing measure before data assimilation (Fig. S2). In instances where multiple retrievals occupy a single model grid box, the data points are aggregated using inverse distance weighting based on grid cell center coordinates. The transformed satellite datasets are processed at a 3-hourly temporal resolution, with each assimilation cycle using observations from the preceding 3-hour window. For example, the 03:00 UTC analysis uses observations collected between 00:00 to 03:00 UTC. The analysis is executed at 3-hour intervals, and no interpolation is applied to grid cells without observations. Preprocessing is carried out independently for each of the four satellite sensors. This transformation of satellite data onto the model grid provides two key advantages: data thinning, which reduces redundancy, and enhanced computational efficiency, both of which contribute to an optimized assimilation process. For ESA-CCI, which is provided as a daily mean product, the data are adapted to the 3-hourly framework by assigning the

https://doi.org/10.5194/egusphere-2026-4240
Preprint. Discussion started: 14 August 2026

observations to the 00:00–03:00 LT window. This choice reflects that daily mean SM is most representative of conditions near 00 LST and avoids introducing biases associated with diurnal variability.

2.5 Data assimilation experiments

This study conducts a comprehensive set of trials involving both individual and combined sensor inputs for SM DA. The single-sensor DA experiments separately assimilate each satellite dataset into the JULES LSM, denoted as DA(SMAP), DA(SMOS), DA(ASCAT), and DA(AMSR2), respectively. The multi-sensor SM assimilation system, denoted as DA(Multi), integrates observations from all four sensors: SMAP, SMOS, ASCAT, and AMSR2. For comparison, we also assimilate the multi-sensor retrievals from the ESA-CCI SM product (hereafter DA(CCI)), as this comparison is important from multiple perspectives. It allows us to evaluate whether the benefits of multi-sensor assimilation are consistently reproduced using an independent multi-sensor dataset. This benchmark also enables us to examine the extent of improvement when a larger number of sensors included in ESA-CCI are integrated. Furthermore, it serves to examine whether pre-merging observations into a single harmonized SM product prior to data assimilation offers an advantage over explicitly assimilating individual sensor observations within the DA(Multi) framework.

All DA experiments are performed using ensemble size of 12, coupled with a 3-h cycling interval. The 3-hourly outputs are used for sub-daily assessments and aggregated to the daily values for daily data validations. The Openloop simulation, used as a reference, adopts an ensemble size identical to the DA experiments and serves as the baseline for evaluating skill improvements. The Openloop is an LSM simulation that runs continuously throughout the year, including the boreal winter period. The DA experiments are conducted for the boreal warm season period of April-September of each year from 2015 to 2021, with the ensemble members initialized from the Openloop simulation on April 1 of each year. Validation focuses on May-September, minimizing the influence of frozen soil and snow cover and allowing for a consistent evaluation of SM DA performance.

2.6 Validation strategy

This study employs the Instrumental Variable (IV) approach (Su et al., 2014) to evaluate improvements achieved by DA in terms of the temporal correlation (R) calculated for soil moisture anomalies. SM anomalies are calculated as the deviation of the raw observations from their respective multi-year monthly climatology. The IV method enables the skill assessment of surface SM products by correlating the estimates with independent but imperfect satellite observations. To reduce bias in skill assessment due to random measurement errors, the method utilizes the temporal persistence of SM by using a lagged version of the same satellite dataset as the instrument. Since DA(Multi) assimilates all single-sensor datasets and DA(CCI) assimilates a multi-sensor retrieval product, independent observations are not available for these experiments; therefore, only the single-sensor DA experiments are validated using the IV method. QC is applied to ensure consistency between satellite and model data, excluding any locations where R < 0.1 for either the Openloop or any DA experiment, following the approach of (Fox et al., 2025) (see Supplementary Information for details). This filtering ensures instrument validity and avoids instability in the statistical estimators.

Assimilation skill is quantified relative to the Openloop simulation using the change in R (ΔR) and the change in the unbiased root-mean-square difference (ΔubRMSD)(Entekhabi et al., 2010a), defined as the difference between the respective performance metrics of the DA experiment and the Openloop. Detailed assessments of Bias, RMSD, and R for the raw data (that is, without removing the mean seasonal cycle) are provided in Fig. S8. For the sub-daily validation presented in Sect. 3.4, both the assimilated SM and the in-situ observations are taken from the preceding 3-hour interval, with the analysis conducted at 00:00, 03:00, 06:00, 09:00, 12:00, 15:00, 18:00, and 21:00 UTC. For convenience, LT is defined as UTC for Europe and UTC minus 6 for North America. (In East Asia, validation is possible only at the daily scale; Sect. 2.2.) Validation is performed by comparing analyses and observations from corresponding time slots only.

3 Results

3.1 Spatiotemporal coverage in satellite retrievals

This section analyzes the number of observations that are available for assimilation from multiple sensors in terms of the global spatiotemporal distribution of SM observations. The ratio of observations assimilated in the multi-sensor configuration relative to the SMAP-only run is shown in Fig. 1a. In the global average, the multi-sensor product ingests 4.47 times as many observations as does the SMAP DA experiment. Regionally, the ratios are 4.56 over North America (30°-50°N, 130°-80°W), 5.38 over Europe (35°-60°N, 10°W-20°E), and 4.05 over East Asia (25°-50°N, 75°-135°E). In the Northern Hemisphere (NH), the relative observation count is highest over mid-latitude regions, particularly in central North America, portions of Western and Central Europe, interior Eurasia, and eastern China. This regional variation arises from differences in the swaths of polar-orbiting satellites and the resulting spatiotemporal sampling characteristics. Localized high ratios (>7) in the figure correspond to regions where SMAP sampling is limited due to topographical complexity.

Figure 1b illustrates the percentage of the global land area covered by the assimilated observations from each sensor, stacked up within each 3-hourly DA cycle. SMAP and SMOS combined provide observations over approximately 13% of the global land at 06:00 and 18:00 LT, respectively, ASCAT samples about 6% at 00:00 and 12:00 LT, and AMSR2 covers about 10% at 03:00 LT and 15:00 LT. These sampling percentages are determined not only by the orbital geometry and swath width of each sensor but also by the filtering applied during quality control. As noted earlier, the higher number of SMOS observations compared to SMAP at 06:00 and 18:00 LT results from the inclusion of all SMOS data without applying RFI filtering. While single-sensor assimilation limits coverage to the local overpass times of the assimilated sensor, combining multiple sensors provides coverage across multiple sub-daily sampling windows. Within the 3-hour DA cycle, this multi-sensor integration greatly increases the density and frequency of available observations, substantially improving both spatial and temporal coverage.

https://doi.org/10.5194/egusphere-2026-4240
Preprint. Discussion started: 14 August 2026

The spatiotemporal sampling characteristics of each satellite are illustrated in Fig. S3, which shows the spatial distribution of SMAP, SMOS, ASCAT, and AMSR2 observations over global land from 2 May 2015, 21:00 UTC to 3 May 2015, 00:00 UTC. This demonstrates the distinct sampling patterns of each satellite associated with its orbital geometry. The multi-sensor assimilation experiment integrates these fragmented observations into a substantially broader and more continuous spatial coverage, demonstrating the benefit of merging multiple data sources to overcome the limitations of individual sensors. Since SM retrievals are routinely integrated into land surface modelling schemes to improve hydrological state estimates at sub-daily spatiotemporal scales, such multi-sensor integration is expected to enhance the overall quality of SM estimates.

3.2 Skill of SM estimates from single-sensor DA experiments over the globe

This section evaluates the skill of surface SM estimates from single-sensor DA experiments using the IV approach (Sect. 2.6) at a global scale. Figure 2a displays the R skill of the Openloop simulation. The global mean R skill of the Openloop is 0.47, with regional values of 0.53 (North America), 0.51 (Europe), and 0.52 (East Asia). For the zonal mean, the Openloop presents better skill in the mid-latitudes than near the equator. The primary driver of the Openloop skill is influenced by the accuracy of the near-surface atmospheric drivers, which tends to be higher in mid-latitudes than in the tropics because there are typically better atmospheric observing systems in the mid-latitudes and thus better surface meteorological forcing data. The regional differences in Openloop performance are also closely linked to land cover. Higher skill over central North America and the Eurasian Steppe likely reflects the predominance of less complex vegetation types (e.g., crop, grass, and shrubland) and more favorable soil properties, which enable the system to accurately reflect the sensitivity of soil moisture to meteorological drivers.

The Openloop simulation serves as a baseline for DA performance verification, and Fig. 2b shows ΔR averaged across the four single-sensor DA experiments (each shown individually in Fig. S4). Averaged globally, the R skill improves by 0.045. Skill improvements are observed across most land regions, with notable gains in central North America, where Openloop performance is already high. The averaged ΔR is 0.038 in North America, 0.026 in Europe, and 0.043 in East Asia, indicating that satellite DA consistently enhances surface SM performance in all three major regions. The African region shows a relatively high ΔR compared to other regions. This enhancement appears to be associated with the weaker performance of the Openloop, likely caused by the lower quality of precipitation data in this area. The zonally averaged ΔR reveals positive values in the equatorial region, where the baseline model skill is low, and in the NH mid-latitudes, where the baseline skill is relatively high. This suggests that satellite DA is effective not only in correcting substantial model deficiencies in poorly performing regions but also in further enhancing SM estimates where the model already performs well. Positive ΔR values are observed across most land-cover types, with the largest improvement in savanna regions where the Openloop performance is comparably low. Significant gains also occur in grasslands, despite the relatively high baseline skill, whereas forests and shrublands show small improvements, likely due to signal attenuation caused by dense vegetation.

https://doi.org/10.5194/egusphere-2026-4240
Preprint. Discussion started: 14 August 2026

An analysis of the skill differences among single-sensor DA experiments is presented in Fig. 2c, which displays the spread between the maximum and minimum R improvements ($\Delta R_{max} - \Delta R_{min}$) across the four single-sensor DA experiments. This metric highlight region where DA skill is highly sensitive to the choice of satellite sensor. Across most NH mid-latitudes, differences among sensors are marginal, but they become more pronounced over parts of East Asia and India. In the zonal mean, skill differences remain small in the mid-latitudes but increase substantially in high-latitude regions. By land cover type, large inter-sensor variations are found in forested and savannah regions, whereas shrub, crop, and grassland areas show relatively small variability. These patterns likely reflect differences in frequency-dependent penetration depth (e.g., L-band vs. C-band) under dense vegetation. Furthermore, the spatial distribution of $\Delta R_{max} - \Delta R_{min}$ (Fig. 2c) shows little correspondence with either the Openloop performance (Fig. 2a) or the averaged skill improvement across the four single-sensor DA experiments (Fig. 2b), with the spatial correlation coefficients with Fig. 2a and 2b below 0.1. This suggests that the relative superiority of a given sensor is not primarily governed by baseline model skill, but rather by sensor-specific observational characteristics and their effectiveness under local environmental conditions.

Figure 2d identifies the single-sensor DA experiment with the best skill in each region. Across the globe, SMAP assimilation provides the highest skill over 48% of land areas, followed by ASCAT (24%), AMSR2 (16%), and SMOS (12%) assimilation. Regionally, DA(SMAP) generally dominates across North America, although ASCAT and AMSR2 contribute notably in the western and north-central regions. In Europe, SMAP again shows superior skills, but AMSR2 exhibits clear advantages in the south, demonstrating regional variability in sensor effectiveness. In East Asia and Eurasia, SMAP remains competitive, while C-band sensors (ASCAT, AMSR2) perform better in several arid regions. L-band sensors (SMAP, SMOS) achieve their greatest advantage in forests and savannas, consistent with their superior penetration through relatively dense vegetation. By contrast, C-band sensors tend to perform relatively better in shrubs and grasslands, possibly due to their sensitivity to the distinct soil and vegetation properties. These regional contrasts in sensor performance demonstrate that relying on a single sensor is almost certainly suboptimal and highlight the promise of multi-sensor approaches for improving global SM analyses.

3.3 Skill improvements in SM assimilation experiments against in-situ measurements

This section compares the skill improvement of the single- and multi-sensor assimilation experiments using in-situ observations across North America, Europe, and East Asia (Sect. 2.2). For the Openloop simulation, R=0.49 on average in North America, with particularly high performance (>0.6) in the central region and lower performance in the west (Fig. 3a). Mean R values are 0.51 in Europe and 0.34 in East Asia (Figs. 3b and c).

In North America, DA(SMAP) improves R by 0.07 on average compared to the Openloop, with notable gains in both the central US, where baseline performance is already high, and the western region, where the skill is lower, although some stations in the central and southern areas show degraded skills (Fig. 3d). Among the single-sensor experiments, DA(SMAP) displays the largest improvement (Fig. 4a), followed by DA(AMSR2) (ΔR~0.05), DA(ASCAT) (ΔR~0.05), and DA(SMOS)

https://doi.org/10.5194/egusphere-2026-4240
Preprint. Discussion started: 14 August 2026

(ΔR~0.01), with ASCAT and AMSR2 showing more pronounced benefits in the western US (not shown). In Europe, DA(SMAP) increases the averaged ΔR by 0.05 relative to the Openloop (Fig. 3e), followed by AMSR2 (ΔR~0.03), ASCAT (ΔR~0.02), and SMOS (ΔR~0.00) (Fig. 4b). In East Asia, DA(SMAP) again yields the significant improvement (ΔR~0.13; Fig. 3f), closely followed by ASCAT (ΔR~0.11), AMSR2 (ΔR~0.06), SMOS (ΔR~0.06) (Fig. 4c). Despite regional dependency, all single-sensor experiments consistently improve the skill across North America, Europe, and East Asia, underscoring the potential of multiple sensor datasets for enhancing SM estimates through DA.

To assess the added value of multi-sensor assimilation, DA(Multi) is compared with DA(SMAP), which provides the highest skill among the single-sensor systems. DA(Multi) provides additional skill enhancement over DA(SMAP) across most regions (Figs. 3g-i). However, the magnitude and spatial pattern of these improvements vary by region. Over North America (Fig. 3g), DA(Multi) shows notable additional improvements compared with DA(SMAP) in the western regions, where the Openloop skill is relatively low. In contrast, skill reductions appear in parts of the central and southeastern regions, where the Openloop and DA(SMAP) already perform relatively well. Similar regional contrasts in skill enhancement are also observed over Europe (Fig. 3h) and East Asia (Fig. 3i). Across the analysis domains in North America, Europe, and East Asia, DA(Multi) increases R skill by 0.01-0.02 beyond DA(SMAP) and consistently outperforms all single-sensor experiments (Fig. 4). As shown in Fig. 2d, the single-sensor system with the highest skill differs regionally. Therefore, the multi-sensor approach demonstrates the potential to yield superior and consistent performance across diverse geographic environments. It is also noted that, although the RFI filtering of SMOS could potentially influence the performance of both DA(SMOS) and DA(Multi), the sensitivity analysis conducted in this study indicates that its impact is negligible (Fig. S6).

Previous studies (Draper et al. 2012; Fox et al. 2025; Lievens et al. 2017; Seo et al. 2021) have demonstrated the capacity of surface data assimilation to propagate information into the deeper root-zone soil layers. Our results confirm this effect, with skill enhancements extending into deeper layers over North America and Europe (Fig. 4; validation not available for East Asia). In North America, all single sensor DA experiments show higher R skill than the Openloop. DA(SMAP) increases R skill by 0.04 over that of the Openloop, outperforming other configurations. The assimilation of other sensors, specifically DA(ASCAT) and DA(SMOS), also outperformed the Openloop simulation by 0.02. DA(Multi) achieves a ΔR of 0.04, comparable to the best single-sensor DA(SMAP), while demonstrating statistically significant improvements in the root zone. In Europe, all single-sensor assimilation experiments surpassed the Openloop performance (0.47). Among the single sensors, DA(SMAP) shows the most substantial improvement with a ΔR of 0.03. Notably, DA(Multi) yields even superior results compared to the single sensors, achieving a ΔR of 0.04.

Evaluation against in-situ observations demonstrates that DA(CCI) consistently provides enhanced performance compared to the Openloop and generally outperforms most single-sensor DA experiments. However, the improvements from DA(CCI) are limited and do not exceed those achieved by DA(Multi), which provides additional R-skill gains of 0.03 (NA), 0.02 (EU), and 0.01 (EA) relative to DA(CCI) (Figs. 4 and S7). While the ESA-CCI product is a highly refined, state-of-the-art dataset incorporating advanced screening and quality control, the expected advantages from integrating a larger number of sensors and applying pre-merging (harmonization) are not fully realized in the assimilation results. This likely related to differences in the representation of observation errors. In DA(Multi), individual sensors are assimilated separately, allowing the LETKF to account for sensor-specific errors. In constrast, ESA-CCI is a blended product, making it difficult to prescribe appropriate observation error statistics for sensors with differing characteristics. As a result, DA(Multi) benefits from preserving sensor identity and enabling sensor-specific error treatment.

The ubRMSD of the SM time series further confirms the effectiveness of assimilation (Fig. 4d -4f). In North America, the Openloop simulation yields a ubRMSD of 0.067 m3 m-3 at the surface and 0.048 m^3 m^{-3} in the root zone. The single-sensor DA experiments reduce ubRMSD by about 0.002–0.008 m^3 m^{-3} at the surface and 0.005–0.011 m^3 m^{-3} in the root zone, while DA(multi) achieves reductions of approximately 0.008 m^3 m^{-3} and 0.013 m^3 m^{-3}, respectively. In Europe, the Openloop ubRMSD is around 0.055 m^3 m^{-3} (surface) and 0.047 m^3 m^{-3} (root zone), with DA experiments yielding modest reductions of about 0.001–0.003 m^3 m^{-3}. Similarly, in East Asia, the Openloop ubRMSD is approximately 0.061 m^3 m^{-3}, and reductions from DA experiments range from about 0.002 to 0.007 m^3 m^{-3}. Although these improvements are generally small and not statistically significant in Europe and East Asia, they consistently indicate reduced errors relatively to the Openloop. Notably, the impact of SMOS is particularly distinct, contributing to the error reduction. Overall, the multi-sensor DA consistently demonstrates superior skills in both R and ubRMSD relative to the Openloop and single-sensor systems, highlighting its value in producing more accurate and reliable SM estimates. While both single- and multi-sensor DA generally reduce RMSD across all regions, most improvements are not statistically significant in Europe and East Asia. A notable exception is DA(SMOS) in North America, which shows significant improvements in both RMSD and BIAS. Overall, BIAS exhibits little change across most configurations (Fig. S8).

3.4 Skill improvements at the sub-daily time scale

This study employs a 3-hourly DA cycle, and because the satellites have different orbital paths and local overpass times, the multi-sensor DA incorporates an increased density of measurements per analysis step. This offers spatiotemporal advantages at the sub-daily scale, and this section examines the benefits of the multi-sensor assimilation at the sub-daily scale. The sub-daily validation is conducted based on the R at each 3-hour temporal resolution. As detailed in Table S1, the configuration of both spaceborne retrievals and ground-based recordings is determined by data from the previous 3-hour period, and the analysis represents at each 3-hourly time step. The locations of in-situ network stations in North America and Europe used for the sub-daily analysis are shown in Fig. S5. Across both North America and Europe, the validation results show consistent patterns throughout the study period, with no substantial differences attributable to variations in the number of samples (cf. Figs. 3 and S5).

DA (SMAP) outperforms the Openloop across all sub-daily intervals. Relatively large enhancements in predictive skill were evident across both surface and root-zone soil moisture states. around 06:00 and 18:00 LT, corresponding to the SMAP overpass times (Figs. 5a and 5c), whereas the improvements diminish slightly during other times when no direct assimilation is conducted. This reflects the limited effectiveness of single-sensor systems that update the analysis only at fixed times.

https://doi.org/10.5194/egusphere-2026-4240
Preprint. Discussion started: 14 August 2026

DA(Multi) yields consistent improvements over DA(SMAP) as well as over Openloop throughout the diurnal cycle, showing positive ΔR values against DA(SMAP) during both daytime and nighttime in surface and root-zone estimates (Figs. 5b and 5d). The difference in R skill at each time likely arises from the combined effects of diurnal variations in the Openloop performance and the time-varying contributions of different satellite sensors at their respective overpass times. The Openloop exhibits relatively higher skill between 06:00 and 12:00 LT, followed by a decline until 18:00 LT, and it recovers by 03:00 LT. Overall, DA(Multi) compensates for weaknesses in the Openloop simulations, particularly during the evening hours around 18:00 LT, and maximizes the assimilation benefits in both surface and root-zone SM, enabling a more complete representation of diurnal SM variation.

DA(Multi) shows consistent performance improvements over DA(SMAP) during both daytime and nighttime, while the variations at individual time steps reflect the differing contributions of each satellite sensor. To further illustrate these aspects, we compare the skill differences between DA(Multi) and DA(SMAP) across 3-hourly local times (Fig. 6a). The combined assimilation of SMAP and SMOS produces a pronounced skill gain at 06:00 LT compared with SMAP assimilation alone, owing to the better relative performance of both sensor observations against the Openloop (Fig.6c), whereas the skill declines at 09:00 LT when no satellite observations are assimilated. At 12:00 LT, skill increases due to ASCAT observations from the 09:30 LT overpass, reflecting the relatively better performance of this sensor (Fig. 6c). At 15:00 LT, the assimilation of AMSR2 observations in DA(Multi) yields the greatest skill improvement relative to DA(SMAP), occurring just before the 18:00 LT SMAP assimilation when DA(SMAP) reaches its minimum skill, thereby reflecting the added benefits of assimilating other sensors in DA(Multi). At 18:00 LT, the improvement over DA(SMAP) is lower than at the previous time, and SMOS assimilation adds less benefit since SMAP is also assimilated and already provides strong skill. Nonetheless, additional improvements are found in root-zone SM, highlighting the indirect benefits of multi-sensor assimilation for SM estimation in deeper layers. At 21:00 LT, the relative skill improvement in DA(Multi) decreases, because no satellite observations are assimilated. Then, ASCAT adds the skill slightly at 00:00 LT, but not substantially due to weaker performance. Since the backscatter signal in ASCAT is sensitive not only to SM but also to vegetation moisture, which can interfere with SM retrievals, it tends to be stronger at night due to nocturnal leaf rehydration and weaker during the day from vegetation water loss (Lei et al. 2015; Schroeder et al. 2016). Relative performance peaks at 03:00 LT with AMSR2 assimilation, for which single-sensor DA(AMSR2) performs better at night than during the day (Figs. 6b and 6c). As a passive microwave sensor, AMSR2 is less effective during daytime because soil–vegetation temperature differences complicate the SM retrieval. This consistency reinforces the evidence presented by previous investigations (Parinussa et al., 2011b). These results highlight how the satellites complement each other in determining the effectiveness of multi-sensor assimilation at sub-daily timescales.

https://doi.org/10.5194/egusphere-2026-4240
Preprint. Discussion started: 14 August 2026

4 Conclusion

This study assimilates SM data from multiple sensors SMAP, SMOS, ASCAT, and AMSR2 into the JULES LSM over seven boreal warm seasons (May–September of 2015–2021). By combining the unique orbital characteristics and overpass times of each satellite, the multi-sensor assimilation overcomes the limitations of single-sensor assimilation systems and significantly reduces the spatiotemporal gaps in SM observation. Assimilated surface SM estimates are validated globally using the IV approach. Moreover, assimilated surface and root-zone SM is validated against in-situ measurements in North America, Europe, and East Asia (surface SM only in East Asia). The present study quantitatively evaluates multi-sensor DA by demonstrating how it complements the LSM and overcomes the limitations of single-sensor systems at a sub-daily scale, which provides a framework for advancing the SM DA framework.

The IV-based evaluation shows that single-sensor DA consistently improves surface SM estimates relative to the Openloop run, yet the magnitude of those improvements varies across regions and land-cover types. SMAP generally provides the strongest gains, particularly over mid-latitude cropland and grassland, while ASCAT and AMSR2 yield localized advantages in shrublands, arid regions, and parts of southern Europe. In contrast, improvements are generally smaller in forest and savanna regions, reflecting the differing sensitivities of L- and C-band sensors to vegetation and soil properties. These results confirm that no single-sensor DA system is universally optimal, highlighting the value of a multi-sensor assimilation framework that leverages the complementary strengths of multiple microwave satellite observations.

Validation against in-situ observations further supports this conclusion. The multi-sensor DA system consistently outperforms single-sensor systems across North America, Europe, and East Asia, yielding additional gains in anomaly correlation. Benefits extend to the root zone as well, though improvements there are smaller than at the surface. While SMAP remains a cornerstone dataset, the assimilation of multiple microwave sensors offers the most robust and scalable approach to advancing both surface and root-zone SM analyses.

The additional DA(CCI) experiment consistently demonstrates that the use of multi-sensor observations leads to overall skill improvements. However, the finding that DA(Multi) generally outperforms DA(CCI) suggests that the explicit characterization of sensor-specific uncertainties within the DA framework is as critical to skill improvements as the use of multiple sensors itself. While ESA-CCI represents a state-of-the-art integration of multiple satellites, its effectiveness in global data assimilation can be limited when a single, constant observation error is prescribed for a blended product composed of sensors with diverse characteristics. In contrast, the DA(Multi) framework assimilates observations from individual sensors separately, enabling the explicit specification of sensor-specific observation errors. By accounting for these distinct uncertainty characteristics, the LETKF can more effectively weight each retrieval, leading to a more physically consistent and refined soil moisture analysis. Although the higher temporal resolution of DA(Multi) may also play a role, the primary advantage of DA(Multi) over pre-merged products likes in its ability to optimize the contribution of each sensor through tailored error statistics. This approach ultimately improves the representation of soil moisture and enhances the system’s ability to capture hydrological responses to short-term atmospheric forcing.

When the skill of assimilated SM estimates is validated at sub-daily timescales, improvements in single-sensor DA are limited to the specific overpass times within the 3-hourly cycle. DA(Multi) improves the performance of 3-hourly SM estimates, providing consistent gains during both daytime and nighttime. Even at 06:00 and 18:00 LT, when SMAP is assimilated, DA(Multi) incorporates additional SMOS observations, further increasing skill compared with DA(SMAP). The relatively better performance of passive sensors (AMSR2) at nighttime and active sensors (ASCAT) during the daytime, compared with the Openloop, contributes to the overall skill increase by multi-sensor DA at sub-daily timescales. This approach can improve the representation of diurnal dynamics of land surface processes and ultimately enables the development of more advanced sub-daily land surface reanalyses.

These improvements through the multi-sensor DA system are especially critical for operational forecast centers, where forecasts are issued multiple times per day, since advanced sub-daily land initialization can reduce prediction gaps associated with forecast start times. Beyond advancing forecast systems, the improved SM datasets will not only provide the best-available estimates but also serve as essential inputs for understanding land surface processes and their coupling with the atmosphere, supporting drought monitoring, and improving land initialization in numerical weather prediction and climate models.

Acknowledgements

This work was funded by the Korea Meteorological Administration Research and Development Program under Grant RS-2025-02313090. Sunlae Tak & Eunkyo Seo were supported by Global - Learning & Academic research institution for Master's·PhD students, and Postdocs (LAMP) Program of the National Research Foundation of Korea (NRF) grant funded by the Ministry of Education (No. RS-2023-00301702). Rolf Reichle was supported by the NASA SMAP mission.

Data availability

ISMN are available in their website (https://ismn.earth/en/data/data-download). Soil moisture retrievals from SMAP (https://nsidc.org/data/smap/data), SMOS (https://smos-diss.eo.esa.int/oads/access/), ASCAT (https://archive.eumetsat.int/), and AMSR2 (https://search.earthdata.nasa.gov/) are available to each website, respectively. ESA-CCI v09.2 can be accessed from the website (https://data.ceda.ac.uk/neodc/esacci/soil_moisture/data/daily_files). MODIS land cover can be accessed from the NASA EARTHDATA website (https://doi.org/10.5067/MODIS/MCD12Q2.006)

Code availability

The source code for the analysis and visualization and datasets is available at (https://doi.org/10.5281/zenodo.21040815)

https://doi.org/10.5194/egusphere-2026-4240
Preprint. Discussion started: 14 August 2026

Author contributions

Conceptualization: ST, ES, ML, and RR. Investigation, methodology, and formal analysis: ST, ES, ML. Writing (original draft preparation): ST. Writing (review and editing): ST, ES, ML, and RR.

Competing interests

The contact author has declared that neither of the authors has any competing interests.

References

Aonashi, K., Awaka, J., Hirose, M., Kozu, T., Kubota, T., Liu, G., Shige, S., Kida, S., Seto, S., Takahashi, N., and Takayabu, Y. N.: GSMaP Passive Microwave Precipitation Retrieval Algorithm : Algorithm Description and Validation, Journal of the Meteorological Society of Japan. Ser. II, 87A, 119–136, https://doi.org/10.2151/jmsj.87A.119, 2009.

Azimi, S., Dariane, A. B., Modanesi, S., Bauer-Marschallinger, B., Bindlish, R., Wagner, W., and Massari, C.: Assimilation of Sentinel 1 and SMAP–based satellite soil moisture retrievals into SWAT hydrological model: the impact of satellite revisit time and product spatial resolution on flood simulations in small basins, Journal of hydrology, 581, 124367, https://doi.org/10.1016/j.jhydrol.2019.124367, 2020.

Barnett, T. P., Adam, J. C., and Lettenmaier, D. P.: Potential impacts of a warming climate on water availability in snow-dominated regions, Nature, 438, 303–309, https://doi.org/10.1038/nature04141, 2005.

Bateni, S. M. and Entekhabi, D.: Relative efficiency of land surface energy balance components, Water Resources Research, 48, https://doi.org/10.1029/2011wr011357, 2012.

Beck, H. E., Pan, M., Miralles, D. G., Reichle, R. H., Dorigo, W. A., Hahn, S., Sheffield, J., Karthikeyan, L., Balsamo, G., Parinussa, R. M., van Dijk, A. I. J. M., Du, J., Kimball, J. S., Vergopolan, N., and Wood, E. F.: Evaluation of 18 satellite- and model-based soil moisture products using in situ measurements from 826 sensors, Hydrology and Earth System Sciences, 25, 17–40, http://doi.org/10.5194/hess-25-17-2021, 2021.

Berg, A., Findell, K., Lintner, B., Giannini, A., Seneviratne, S. I., van den Hurk, B., Lorenz, R., Pitman, A., Hagemann, S., Meier, A., Cheruy, F., Ducharne, A., Malyshev, S., and Milly, P. C. D.: Land–atmosphere feedbacks amplify aridity increase over land under global warming, Nature Climate Change, 6, 869–874, https://doi.org/10.1038/nclimate3029, 2016.

Best, M. J., Pryor, M., Clark, D. B., Rooney, G. G., Essery, R. L. H., Ménard, C. B., Edwards, J. M., Hendry, M. A., Porson, A., Gedney, N., Mercado, L. M., Sitch, S., Blyth, E., Boucher, O., Cox, P. M., Grimmond, C. S. B., and Harding, R. J.: The Joint UK Land Environment Simulator (JULES), model description – Part 1: Energy and water fluxes, Geoscientific Model Development, 4, 677–699, https://doi.org/10.5194/gmd-4-677-2011, 2011.

Chan, S. K., Bindlish, R., O'Neill, P. E., Njoku, E., Jackson, T., Colliander, A., Chen, F., Burgin, M., Dunbar, S., Piepmeier, J., Yueh, S., Entekhabi, D., Cosh, M. H., Caldwell, T., Walker, J., Wu, X., Berg, A., Rowlandson, T., Pacheco, A., McNairn, H., Thibeault, M., Martinez-Fernandez, J., Gonzalez-Zamora, A., Seyfried, M., Bosch, D., Starks, P., Goodrich, D., Prueger, J., Palecki, M., Small, E. E., Zreda, M., Calvet, J.-C., Crow, W. T., and Kerr, Y.: Assessment of the SMAP Passive Soil Moisture Product, IEEE Transactions on Geoscience and Remote Sensing, 54, 4994–5007, https://doi.org/10.1109/tgrs.2016.2561938, 2016.

Cho, E., Moon, H., and Choi, M.: First Assessment of the Advanced Microwave Scanning Radiometer 2 (AMSR2) Soil Moisture Contents in Northeast Asia, J Meteorol Soc Jpn, 93, 117–129, https://doi.org/10.2151/jmsj.2015-008, 2015.

De Lannoy, G. J. and Reichle, R. H.: Assimilation of SMOS brightness temperatures or soil moisture retrievals into a land surface model, Hydrology and Earth System Sciences, 20(12), 4895–4911, https://doi.org/10.5194/hess-20-4895-2016, 2016.

Dorigo, W. A., Scipal, K., Parinussa, R. M., Liu, Y. Y., Wagner, W., De Jeu, R. A., and Naeimi, V.: Error characterisation of global active and passive microwave soil moisture datasets, Hydrology and Earth System Sciences, 14(12), 2605–2616, https://doi.org/10.5194/hess-14-2605-2010, 2010.

Draper, C. S., Reichle, R. H., De Lannoy, G. J. M., and Liu, Q.: Assimilation of passive and active microwave soil moisture retrievals, Geophysical Research Letters, 39, https://doi.org/10.1029/2011gl050655, 2012.
Draper, D. W., Newell, D. A., Wentz, F. J., Krimchansky, S., and Skofronick-Jackson, G. M.: The Global Precipitation Measurement (GPM) Microwave Imager (GMI): Instrument Overview and Early On-Orbit Performance, IEEE Journal of Selected Topics in Applied Earth Observations and Remote Sensing, 8, 3452–3462, https://doi.org/10.1109/jstars.2015.2403303, 2015.
Entekhabi, D., Reichle, R. H., Koster, R. D., and Crow, W. T.: Performance Metrics for Soil Moisture Retrievals and Application Requirements, Journal of Hydrometeorology, 11, 832–840, https://doi.org/10.1175/2010jhm1223.1, 2010a.
Entekhabi, D., Njoku, E. G., O'Neill, P. E., Kellogg, K. H., Crow, W. T., Edelstein, W. N., Entin, J. K., Goodman, S. D., Jackson, T. J., Johnson, J., Kimball, J., Piepmeier, J. R., Koster, R. D., Martin, N., McDonald, K. C., Moghaddam, M., Moran, S., Reichle, R., Shi, J. C., Spencer, M. W., Thurman, S. W., Tsang, L., and Van Zyl, J.: The Soil Moisture Active Passive (SMAP) Mission, Proceedings of the IEEE, 98, 704–716, https://doi.org/10.1109/jproc.2010.2043918, 2010b.
Fox, A. M., Reichle, R. H., and Liu, Q.: Assimilation of ASCAT Soil Moisture and SMAP Brightness Temperature Observations into the NASA GEOS Land Data Assimilation System, Journal of Hydrometeorology, 1.aop, https://doi.org/10.1175/JHM-D-24-0139.1, 2025.
Friedl, M. A., Sulla-Menashe, D., Tan, B., Schneider, A., Ramankutty, N., Sibley, A., and Huang, X.: MODIS Collection 5 global land cover: Algorithm refinements and characterization of new datasets, Remote sensing of Environment, 114(1), 168–182, https://doi.org/10.1016/j.rse.2009.08.016, 2010.
Gruber, A., Scanlon, T., Van Der Schalie, R., W., W.,, and Dorigo, W.: Evolution of the ESA CCI Soil Moisture climate data records and their underlying merging methodology, Earth System Science Data, 11(2), 717–739, https://doi.org/10.5194/essd-11-717-2019, 2019.
Halder, S. and Dirmeyer, P. A.: Sensitivity of Numerical Weather Forecasts to Initial Soil Moisture Variations in CFSv2, Weather and Forecasting, 31, 1973–1983, https://doi.org/10.1175/waf-d-16-0049.1, 2016.
Heyvaert, Z., Scherrer, S., Bechtold, M., Gruber, A., Dorigo, W., Kumar, S., and De Lannoy, G.: Impact of Design Factors for ESA CCI Satellite Soil Moisture Data Assimilation over Europe, Journal of Hydrometeorology, 24, 1193–1208, https://doi.org/10.1175/jhm-d-22-0141.1, 2023.
Hunt, B. R., Kostelich, E. J., and Szunyogh, I.: Efficient data assimilation for spatiotemporal chaos: A local ensemble transform Kalman filter, Physica D: Nonlinear Phenomena, 230, 112–126, https://doi.org/10.1016/j.physd.2006.11.008, 2007.
Karthikeyan, L., Pan, M., Wanders, N., Kumar, D. N., and Wood, E. F.: Four decades of microwave satellite soil moisture observations: Part 1. A review of retrieval algorithms, Advances in Water Resources, 109, 106–120, https://doi.org/10.1016/j.advwatres.2017.09.006, 2017.
Kerr, Y. H., Waldteufel, P., Richaume, P., Wigneron, J. P., Ferrazzoli, P., Mahmoodi, A., Bitar, A. A., Cabot, F., Gruhier, C., Juglea, S. E., Leroux, D., Mialon, A., and Delwart, S.: The SMOS soil moisture retrieval algorithm, IEEE transactions on geoscience and remote sensing, 50(5), 1384–1403, https://doi.org/10.1109/TGRS.2012.2184548, 2012.
Kim, H., Lakshmi, V., Kwon, Y., and Kumar, S. V.: First attempt of global-scale assimilation of subdaily scale soil moisture estimates from CYGNSS and SMAP into a land surface model, Environmental Research Letters, 16, https://doi.org/10.1088/1748-9326/ac0ddf, 2021.
Kobayashi, S., Ota, Y., Harada, Y., Ebita, A., Moriya, M., Onoda, H., Onogi, K., Kamahori, H., Kobayashi, C., Endo, H., Miyaoka, H., and Takahashi, K.: The JRA-55 reanalysis: General specifications and basic characteristics, Journal of the Meteorological Society of Japan. Ser. II, 93(1), 5–48, https://doi.org/10.2151/jmsj.2015-001, 2015.
Konapala, G., Mishra, A. K., Wada, Y., and Mann, M. E.: Climate change will affect global water availability through compounding changes in seasonal precipitation and evaporation, Nat Commun, 11, 3044, https://doi.org/10.1038/s41467-020-16757-w, 2020.
Koster, R. D., Guo, Z., Yang, R., Dirmeyer, P. A., Mitchell, K., and Puma, M. J.: On the Nature of Soil Moisture in Land Surface Models, Journal of Climate, 22, 4322–4335, https://doi.org/10.1175/2009jcli2832.1, 2009.
Koster, R. D., Suarez, M. J., Liu, P., Jambor,, U., B., A.,, Kistler, M., Reichle, R., Rodell, M., and Famiglietti, J.: Realistic Initialization of Land Surface States: Impacts on Subseasonal Forecast Skill, Journal of hydrometeorology, 5(6), 1049–1063, https://doi.org/10.1175/JHM-387.1, 2004.

https://doi.org/10.5194/egusphere-2026-4240
Preprint. Discussion started: 14 August 2026

Kumar, S., Peterslidard, C., Tian, Y., Houser, P., Geiger, J., Olden, S., Lighty, L., Eastman, J., Doty, B., and Dirmeyer, P.: Land information system: An interoperable framework for high resolution land surface modeling, Environmental Modelling & Software, 21, 1402–1415, https://doi.org/10.1016/j.envsoft.2005.07.004, 2006.

Kumar, S., Kolassa, J., Reichle, R., Crow, W., de Lannoy, G., de Rosnay, P., MacBean, N., Girotto, M., Fox, A., Quaife, T., Draper, C., Forman, B., Balsamo, G., Steele-Dunne, S., Albergel, C., Bonan, B., Calvet, J. C., Dong, J., Liddy, H., and Ruston, B.: An Agenda for Land Data Assimilation Priorities: Realizing the Promise of Terrestrial Water, Energy, and Vegetation Observations From Space, Journal of Advances in Modeling Earth Systems, 14, https://doi.org/10.1029/2022MS003259, 2022.

Kumar, S. V., Jasinski, M., Mocko, D. M., Rodell, M., Borak, J., Li, B., Beaudoing, H. K., and Peters-Lidard, C. D.: NCA-LDAS land analysis: Development and performance of a multisensor, multivariate land data assimilation system for the National Climate Assessment, Journal of Hydrometeorology, 20(8), 1571–1593, https://doi.org/10.1175/JHM-D-17-0125.1, 2019.

Li, X., Liu, F., Ma, C., Hou, J., Zheng, D., Ma, H., Bai, Y., Han, X., Vereecken, H., Yang, K., Duan, Q., and Huang, C.: Land Data Assimilation: Harmonizing Theory and Data in Land Surface Process Studies, Reviews of Geophysics, 62(1), e2022RG000801, https://doi.org/10.1029/2022RG000801, 2024.

Lievens, H., Reichle, R. H., Liu, Q., De Lannoy, G. J., Dunbar, R. S., Kim, S. B., Das, N. N., Cosh, M., Walker, J. P., and Wagner, W.: Joint Sentinel-1 and SMAP data assimilation to improve soil moisture estimates, Geophysical research letters, 44(12), 6145–6153, https://doi.org/10.1002/2017GL073904, 2017.

Liu, Q., Reichle, R. H., Bindlish, R., Cosh, M. H., Crow, W. T., de Jeu, R., De Lannoy, G., Huffman, G. J., and Jackson, T. J.: The contributions of precipitation and soil moisture observations to the skill of soil moisture estimates in a land data assimilation system, Journal of Hydrometeorology, 12(5), 750–765, https://doi.org/10.1175/JHM-D-10-05000.1, 2011.

Miyoshi, T. and Yamane, S.: Local Ensemble Transform Kalman Filtering with an AGCM at a T159/L48 Resolution, Monthly Weather Review, 135, 3841–3861, https://doi.org/10.1175/2007mwr1873.1, 2007.

Nichols, N. K.: Mathematical concepts of data assimilation, Data assimilation: making sense of observations, 13–39, https://doi.org/10.1007/978-3-540-74703-1_2, 2010.

Parinussa, R. M., Holmes, T. R., and de Jeu, R. A.: Soil moisture retrievals from the WindSat spaceborne polarimetric microwave radiometer, IEEE Transactions on Geoscience and Remote Sensing, 50(7), 2683–2694, https://doi.org/10.1109/TGRS.2011.2174643, 2011a.

Parinussa, R. M., Holmes, T. R. H., Yilmaz, M. T., and Crow, W. T.: The impact of land surface temperature on soil moisture anomaly detection from passive microwave observations, Hydrology and Earth System Sciences, 15, 3135–3151, https://doi.org/10.5194/hess-15-3135-2011, 2011b.

Parinussa, R. M., Holmes, T. R., Wanders, N., Dorigo, W. A., and de Jeu, R. A.: A preliminary study toward consistent soil moisture from AMSR2, Journal of Hydrometeorology, 16(2), 932–947, https://doi.org/10.1175/JHM-D-13-0200.1, 2015.

Reichle, R. H.: Data assimilation methods in the Earth sciences, Advances in water resources, 31(11), 1411–1418, https://doi.org/10.1016/j.advwatres.2008.01.001, 2008.

Reichle, R. H. and Koster, R. D.: Bias reduction in short records of satellite soil moisture, Geophysical Research Letters, 31, https://doi.org/10.1029/2004gl020938, 2004.

Reichle, R. H., Zhang, S. Q., Liu, Q., Draper, C. S., Kolassa, J., and Todling, R.: Assimilation of SMAP Brightness Temperature Observations in the GEOS Land-Atmosphere Data Assimilation System, IEEE J Sel Top Appl Earth Obs Remote Sens, 14, 10628–10643, https://doi.org/10.1109/jstars.2021.3118595, 2021.

Reichle, R. H., Bosilovich, M. G., Crow, W. T., Koster, R. D., Kumar, S. V., Mahanama, S. P., and Zaitchik, B. F.: Recent advances in land data assimilation at the NASA Global Modeling and Assimilation Office, Data assimilation for atmospheric, oceanic and hydrologic applications, 407–428, https://doi.org/10.1007/978-3-540-71056-1_21, 2009.

Ruf, C. S., Chew, C., Lang, T., Morris, M. G., Nave, K., Ridley, A.,, and Balasubramaniam, R.: A new paradigm in earth environmental monitoring with the cygnss small satellite constellation, Scientific reports, 8(1), 8782, https://doi.org/10.1038/s41598-018-27127-4, 2018.

Seneviratne, S. I., Corti, T., Davin, E. L., Hirschi, M., Jaeger, E. B., Lehner, I., Orlowsky, B., and Teuling, A. J.: Investigating soil moisture–climate interactions in a changing climate: A review, Earth-Science Reviews, 99, 125–161, https://doi.org/10.1016/j.earscirev.2010.02.004, 2010.

Seo, E. and Dirmeyer, P. A.: Understanding the diurnal cycle of land–atmosphere interactions from flux site observations, Hydrology and Earth System Sciences, 26(20), 5411–5429, https://doi.org/10.5194/hess-26-5411-2022, 2022a.

Seo, E. and Dirmeyer, P. A.: Improving the ESA CCI daily soil moisture time series with physically based land surface model datasets using a Fourier time-filtering method, Journal of Hydrometeorology, 23(3), 473–489, https://doi.org/10.1175/JHM-D-21-0120.1, 2022b.

Seo, E., Lee, M.-I., and Reichle, R. H.: Assimilation of SMAP and ASCAT soil moisture retrievals into the JULES land surface model using the Local Ensemble Transform Kalman Filter, Remote Sensing of Environment, 253, https://doi.org/10.1016/j.rse.2020.112222, 2021.

Su, C. H., Ryu, D., Crow, W. T., and Western, A. W.: Beyond triple collocation: Applications to soil moisture monitoring, Journal of Geophysical Research: Atmospheres, 119(11), 6419–6439, https://doi.org/10.1002/2013JD021043, 2014.

Trenberth, K. E., Dai, A., van der Schrier, G., Jones, P. D., Barichivich, J., Briffa, K. R., and Sheffield, J.: Global warming and changes in drought, Nature Climate Change, 4, 17–22, https://doi.org/10.1038/nclimate2067, 2013.

Wagner, W., Hahn, S., Kidd, R., Melzer, T., Bartalis, Z., Hasenauer, S., Figa-Saldaña, J., de Rosnay, P., Jann, A., Schneider, S., Komma, J., Kubu, G., Brugger, K., Aubrecht, C., Züger, J., Gangkofner, U., Kienberger, S., Brocca, L., Wang, Y., Blöschl, G., Eitzinger, J., and Steinnocher, K.: The ASCAT Soil Moisture Product: A Review of its Specifications, Validation Results, and Emerging Applications, Meteorologische Zeitschrift, 22, 5–33, https://doi.org/10.1127/0941-2948/2013/0399, 2013.

Wu, W. Y., Lo, M. H., Wada, Y., Famiglietti, J. S., Reager, J. T., Yeh, P. J., Ducharne, A., and Yang, Z. L.: Divergent effects of climate change on future groundwater availability in key mid-latitude aquifers, Nat Commun, 11, 3710, https://doi.org/10.1038/s41467-020-17581-y, 2020.

Xu, X., Tolson, B. A., Li, J., Staebler, R. M., Seglenieks, F., Haghnegahdar, A., and Davison, B.: Assimilation of SMOS soil moisture over the Great Lakes basin, Remote Sensing of Environment, 169, 163–175, https://doi.org/10.1016/j.rse.2015.08.017, 2015.

Yang, J., Zhang, P., Lu, N., Yang, Z., Shi, J., and Dong, C.: Improvements on global meteorological observations from the current Fengyun 3 satellites and beyond, International Journal of Digital Earth, 5, 251–265, https://doi.org/10.1080/17538947.2012.658666, 2012.

https://doi.org/10.5194/egusphere-2026-4240
Preprint. Discussion started: 14 August 2026

Figure

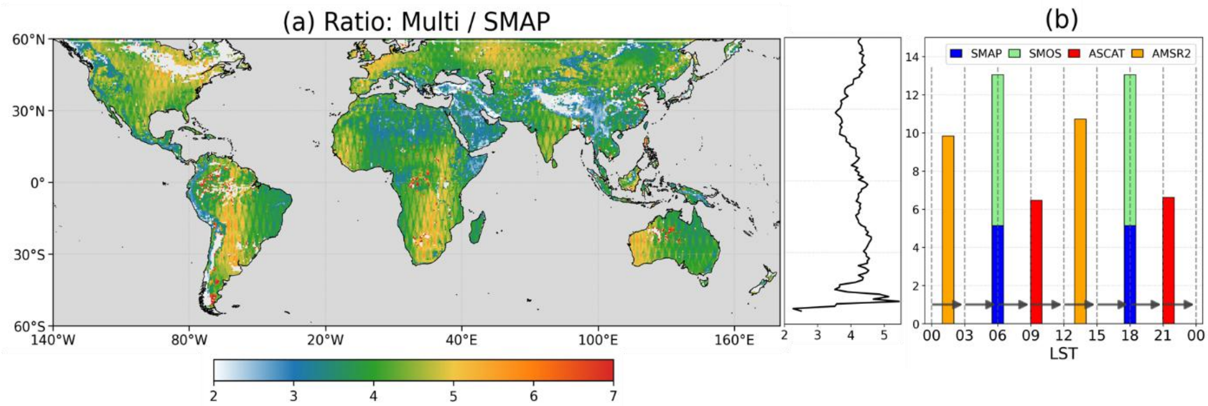

Figure 1: (a) Ratio of the number of SM observations assimilated in the multi-sensor and the SMAP single-sensor systems during the experiment period. The right panel shows the zonal mean across latitude. (b) Percentage of the global land area (excluding Antarctica and Greenland) covered by the assimilated SM observations for each 3-hourly local time (blue: SMAP, light green: SMOS, red: ASCAT, and orange: AMSR2), and vertical dashed lines with arrows (grey) indicate 3-hourly DA cycle.

https://doi.org/10.5194/egusphere-2026-4240
Preprint. Discussion started: 14 August 2026

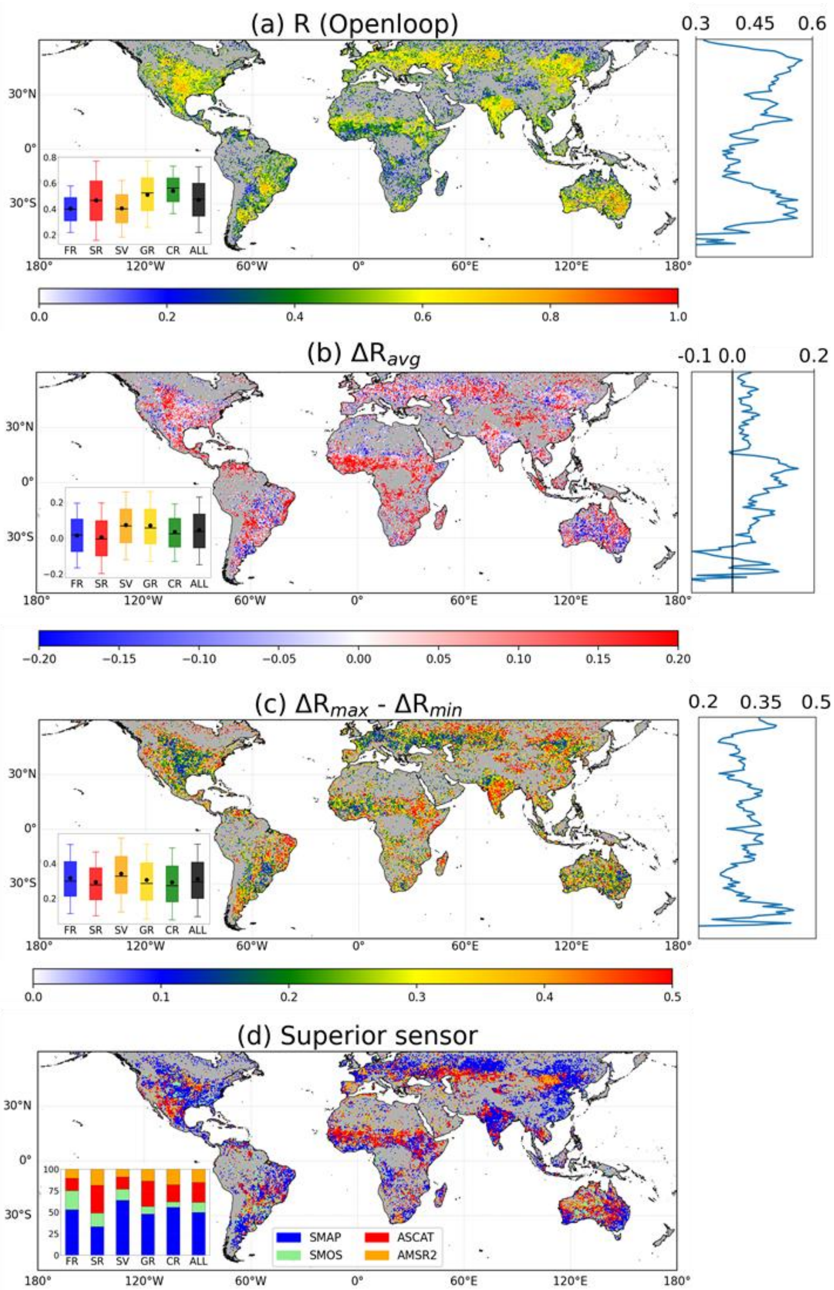

Figure 2: (a) Anomaly temporal correlation (R; dimensionless) of daily surface SM time series for the Openloop simulation; grey shading indicates no-data values owing to insufficient observations. (b) Skill improvement (ΔR) from single-sensor assimilation over the Openloop skill, averaged across the four single-sensor DA experiments. (c) Difference of maximum and minimum ΔR of the four single-sensor experiments. (d) Map of the best-performing single-sensor DA experiment; the cumulative bar graph in the bottom left provides the proportion of best single sensor experiments by land cover type (FR: Forest, SR: Shrub, SV: Savanna, GR: Grassland, CR: Crop). In panels (a)-(c), the zonal mean and breakdown by land cover type are shown in the right and bottom left of each map. The boxplots depict the median and the interquartile range (IQR), defined by the 25th and 75th percentiles. The whiskers are calculated as 0.5 times the IQR from the upper and lower quartiles.

https://doi.org/10.5194/egusphere-2026-4240
Preprint. Discussion started: 14 August 2026

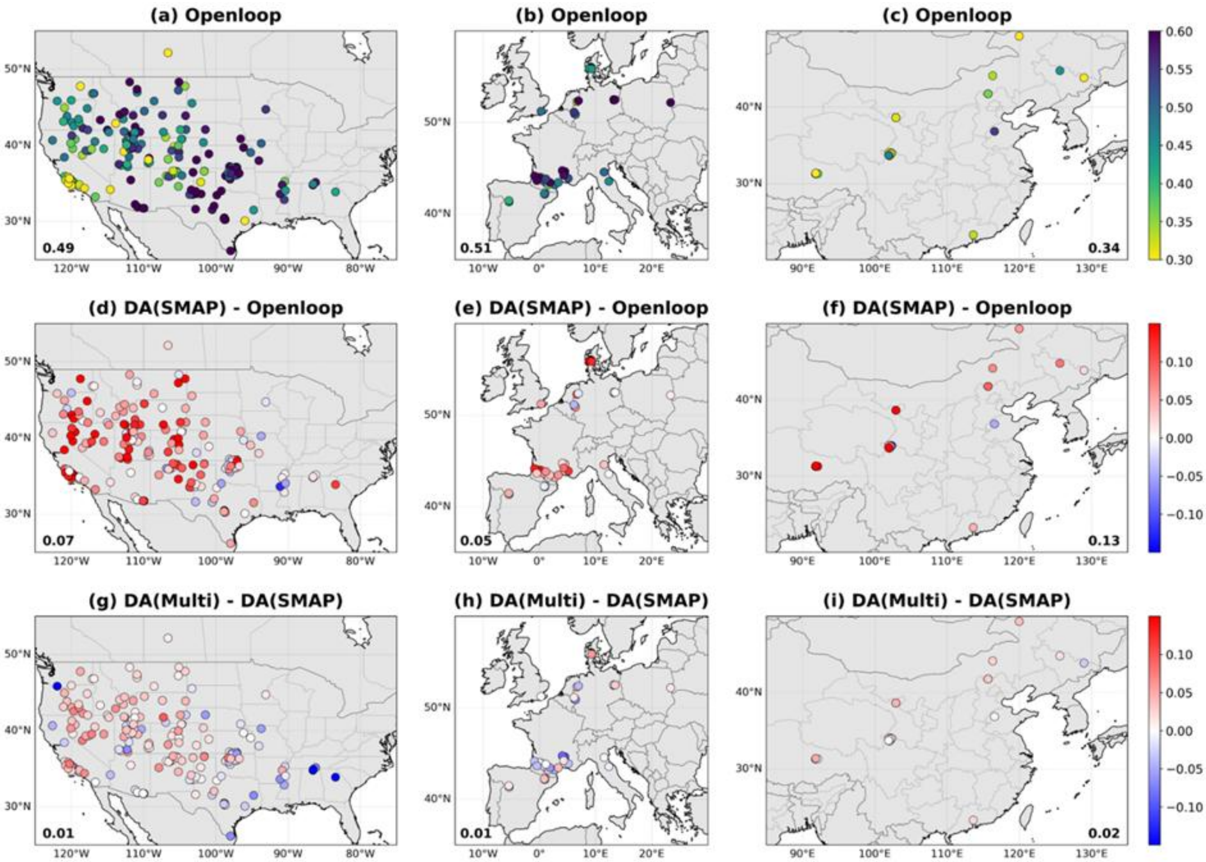

Figure 3: Temporal correlation coefficient of the anomaly time series (R; dimensionless) of surface SM estimates at in-situ sites from the Openloop simulation over (a) North America (N=230), (b) Europe (N=61), and (c) East Asia (N=35). (d-f) Difference in R between DA(SMAP) and Openloop. (g-i) Difference in R between DA(Multi) and DA(SMAP). The spatial average is indicated at the bottom of each figure panel.

https://doi.org/10.5194/egusphere-2026-4240
Preprint. Discussion started: 14 August 2026

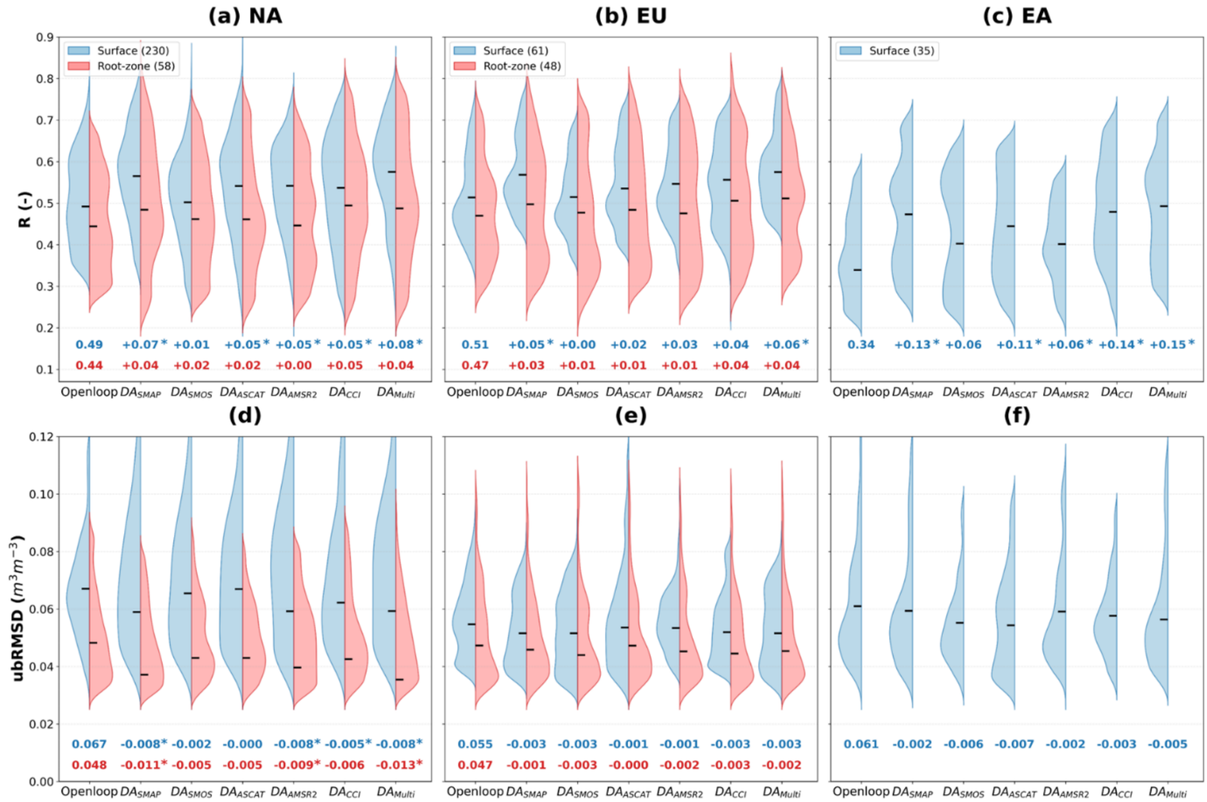

Figure 4: Violin plots of the anomaly correlation coefficient (R; dimensionless) for surface (blue) and root-zone (red) SM from the Openloop simulation and DA experiments, evaluated against in-situ measurements over (a) North America, (b) Europe, and (c) East Asia. The horizontal line in each violin indicates the mean. The values shown at the bottom of the axes indicate the mean metric for the Openloop and, for the DA experiments, the mean difference of the metric from that of the Openloop. Asterisks indicate that the skill improvements in the DA experiments are confirmed to be significant at the 95% confidence interval via the Student's t-test. Numbers in the legend represent the number of stations used for surface and root-zone validation, respectively. Panels (d-f) are the same as panels (a-c), but for the ubRMSD (m^3 m^{-3}).

https://doi.org/10.5194/egusphere-2026-4240
Preprint. Discussion started: 14 August 2026

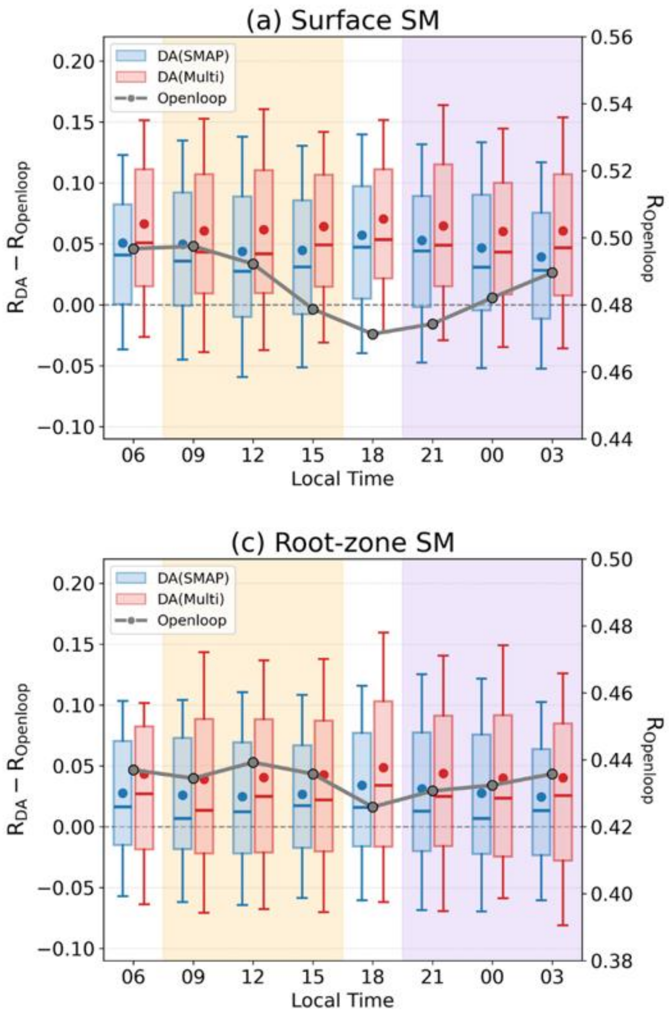

705 **Figure 5: Boxplots of ΔR for DA(SMAP) (blue) and DA(Multi) (red) for (a) surface and (c) root-zone SM across 3-hourly local times, evaluated against in-situ observations over North America and Europe (left y-axis). The grey line indicates the diurnal skill of the Openloop run (right y-axis). Background shading shows daytime (orange; 09:00-15:00 LT) and nighttime (purple; 21:00-03:00 LT). Panels (b) and (d) display daytime- and nighttime-composited skills for surface and root-zone SM, respectively. These boxplots illustrate the IQR (25th–75th percentiles), featuring whiskers that span ±0.5 IQR beyond the quartiles; the horizontal line marks the median, and filled circles denote the mean.**

https://doi.org/10.5194/egusphere-2026-4240
Preprint. Discussion started: 14 August 2026

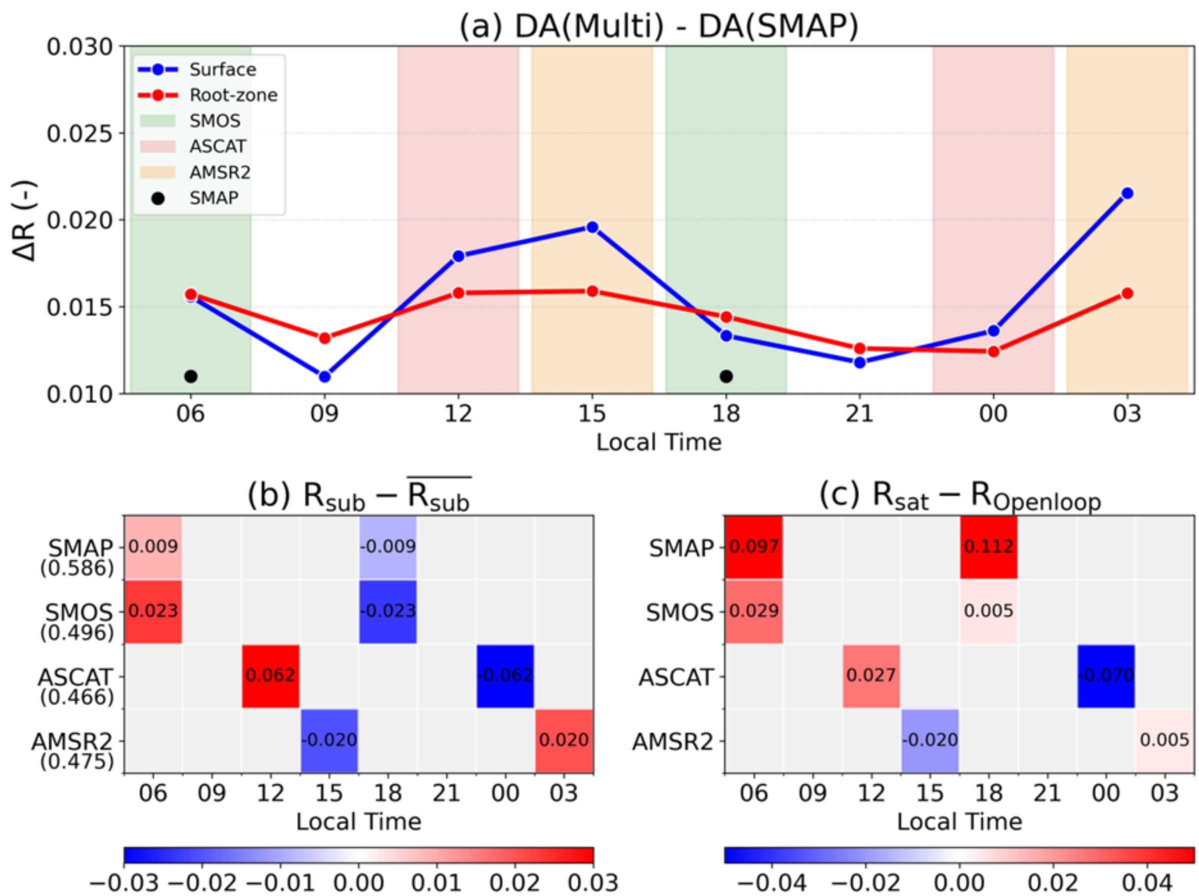

Figure 6: (a) Difference in R (-) between DA(Multi) and DA(SMAP) across 3-hourly local times for surface (blue) and root-zone (red) SM over North America and Europe. Shading indicates the satellite sensors contributing to DA(Multi) within each 3-hour assimilation cycle (green: SMOS, red: ASCAT, and orange: AMSR2), and black dots indicate the local times when SMAP observations are assimilated. (b) Sub-daily skill differences for DA of each sensor across 3-hourly local times, presented relative to their daily DA skill (values shown in parentheses on the y-axis). (c) Differences in correlation between each sensor and in-situ observations relative to the Openloop at sub-daily timescales. Red shading indicates relatively better performance, and blue shading indicates poorer performance compared with the baseline skills in panels (b) and (c).